ISSN 0021-3640, JETP Letters, 2024, Vol. 119, No. 7, pp. 523–528. © The Author(s), 2024. This article is an open access publication.
Russian Text © The Author(s), 2024, published in Pis'ma v Zhurnal Eksperimental'noi i Teoreticheskoi Fiziki, 2024, Vol. 119, No. 7, pp. 518–523.

CONDENSED MATTER

Direct Observation of Pinning of Abrikosov Vortices in a Specially Inhomogenious Crystal $EuRbFe_4As_4$

M. S. Sidelnikov[a,b,*], A. V. Palnichenko[a], K. S. Pervakov[c], V. A. Vlasenko[c], I. I. Zverkova[a], L. S. Uspenskaya[a], V. M. Pudalov[c], and L. Ya. Vinnikov[a]

[a] *Osipyan Institute of Solid State Physics, Russian Academy of Sciences, Chernogolovka, Moscow regoin, 142432 Russia*
[b] *Russian Quantum Center, Moscow, Skolkovo, 121205 Russia*
[c] *Lebedev Physical Institute, Russian Academy of Sciences, Moscow, 119991 Russia*
**e-mail: m.sidelnikov@issp.ac.ru*

Received November 23, 2023; revised February 28, 2024; accepted February 29, 2024

In the two-phase crystal $EuRbFe_4As_4/EuFe_2As_2$ (1144/122), a linear ordering of Abrikosov vortices, uncharacteristic for superconducting pnictides, has been found using the method of decorating with magnetic nanoparticles. The observed chains of vortices directed along crystallographic ⟨110⟩ axes of the orthorhombic $EuFe_2As_2$ phase are explained by pinning of vortices in the superconducting phase 1144 on linear defects associated with the twin boundaries of the non-superconducting 122 phase.

DOI: 10.1134/S0021364024600514

Among iron-based superconductors, the $EuFe_2As_2$-based compounds stand out with a wide range of electronic and magnetic transformations [1]. In particular, one of the interesting objects to study the coexistence of superconductivity and magnetism is the stoichiometric magnetic superconductor $EuRbFe_4As_4$ [2–6] with the superconducting transition temperature $T_{SC} \approx 38$ K and magnetic ordering in the Eu^{2+} layers at $T_M \approx 15$ K. For growing these crystals, the self-flux technique [7] is commonly used. The unit cell of this stoichiometric compound has a c parameter of 1.33 nm and consists of $EuFe_2As_2$ and $RbFe_4As_2$ blocks alternating along the c axis. During crystal growth, the phases 122 and 1144 compete with each other and often the $EuRbFe_4As_4$ compound has an admixture of the parent $EuFe_2As_2$ phase (122) [8], which does not superconduct at ambient pressure, but becomes antiferromagnetic at $T_{AFM} \approx 20$ K. In addition, in $EuFe_2As_2$ there is a structural transition from tetragonal crystal structure ($I4/mmm$) to orthorhombic ($Fmmm$) at temperatures below 200 K, which is accompanied by the emergence of a twin structure and spin ordering of Fe atoms in the spin density wave (SDW) type. By contrast, in $EuRbFe_4As_4$ there is no structural transition, and its crystal structure below room temperature is tetragonal ($P4/mmm$) with primitive Braveau lattice. Previously, the non-superconducting inclusions of the 122 phase were considered only as pinning centers of vortices in the superconducting phase 1144 [8]. In this work, using the decoration technique, we visualized the Abrikosov vortices and studied their distribution. As a result we found a peculiar vortex pinning in the 1144 phase caused by the twin structure of the 122 phase.

The investigated sample was a crystal of $EuRbFe_4As_4$ with dimensions of ≈7 × 5 × 0.25 mm grown by the self-flux technique described in [7, 8]. X-ray diffraction studies of the sample were carried out at room temperature. To check the sample monocrystallinity, an epigram imaging was taken on a URS-2.0 X-ray apparatus with Mo-radiation. A Laue pattern was obtained from the sample with clear point reflexes. In the diffractogram recorded using Rigaku SmartLab SE diffractometer with CuK_α radiation (λ = 1.54178 Å, 40 kV, 35 mA) in the angle interval 2Θ = 3°–130°, two systems of reflection orders were observed, indicating the presence of two phases (Fig. 1a). The lattice parameters of the two phases were 13.30 Å and 12.20 Å, which is in agreement with literature data for $EuRbFe_4As_4$ [9] and $EuFe_2As_2$ [10], respectively. Elemental analysis of the crystal was performed by energy dispersive X-ray spectroscopy (EDX) on a Zeiss Supra 50 VP scanning electron microscope. The analysis carried out in several regions of the crystal surface showed a significant excess of rubidium content on the sample surface: Eu—13.3 ± 1.9, Rb—42.5 ± 8.1, Fe—25.9 ± 3.7, As—18.3 ± 2.6 at %. Magnetic properties were studied by measuring the temperature dependences of the real part of the dynamic magnetic susceptibility $\chi'(t)$ using a laboratory made cryogenic induction magnetometer [11, 12]. The modulating external magnetic field was applied at the frequency of ν = 1500 Hz with the amplitude of

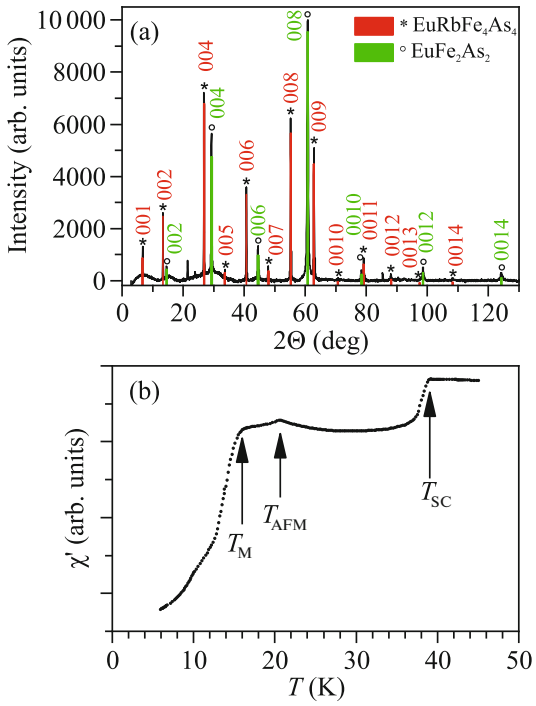

Fig. 1. (Color online) Characterization of the $EuRbFe_4As_4/EuFe_2As_2$ crystal. (a) X-ray diffraction pattern; (b) temperature dependence of the AC magnetic susceptibility with alternating field $H_0 = 3.5$ mOe, $\nu = 1500$ Hz, whereas T_{SC} and T_M correspond to the superconducting and magnetic transition in $EuRbFe_4As_4$, T_{AFM} is the antiferromagnetic transition in $EuFe_2As_2$.

$H_0 = 3.5$ mOe. During the measurements, the orientation of the crystal relative to the magnetic field was arbitrary. The temperature dependence $\chi'(t)$ of the investigated crystal is presented in Fig. 1b. At decreasing temperature, the diamagnetic response of the sample was observed in the region of 39–40 K, corresponding to the temperature of the sample transition to the superconducting state [13]. At a temperature of 21 K, there is a peak in the $\chi'(T)$ dependence characteristic of the transition of 122 phase to the antiferromagnetic state. Subsequent temperature decrease leads to a noticeable drop in $\chi'(T)$ at 15 K associated with magnetic ordering of Eu layers in $EuRbFe_4As_4$ [14].

The magnetic flux structure was visualized using the low-temperature decoration with magnetic nanoparticles [15]—thermal evaporation of iron near the sample in a rarefied helium environment. Abrikosov vortices arising in the crystal in external magnetic field attract iron nanoparticles, therefore distribution of magnetic particles on the crystal surface displays a vortex structure. One of the advantages of the decoration method over other imaging methods is the convenience of studying the magnetic structure of large surface areas with a resolution of up to 100 nm, which is especially important in case of spatially inhomogeneous samples. Prior to observation of the vortex structure the crystal surface was prepared by peeling off the top layers with the adhesive tape. For decoration, the sample immediately after exfoliation was placed in the insert of a filling helium cryostat and cooled in a constant external magnetic field H ("field cooling," FC) to the reference temperature. After that, we performed 2–3 cycles of iron evaporation, which resulted in an incidental heating of the sample by approximately 2–4 K, depending on the duration of the evaporation cycle and the reference temperature. Thus, the sample temperature at the time of decoration was higher than the reference temperature by a random but measurable value. Experiments were performed at temperatures of 8 and 18 K, i.e., both below and above the magnetic ordering temperature in the 1144 phase.

Figure 2a shows an optical microscope image of a fragment of the basal plane *ab* of the studied sample after decoration at $T = 8.2$–8.9 K and $H = 15$ Oe. Clusters of iron nanoparticles are observed, displaying the arrangement of Abrikosov vortices during decoration. The vortices are predominantly lined up in chains along one of the ⟨100⟩ directions of phase 1144, which coincide with the facet boundaries. A closer look at the pattern of vortex distribution highlights several characteristic regions. Figure 2b shows, on an enlarged scale, the region in which the distance between neighboring chains varies. The average distance between close chains is 1.05 μm, while the average distance between more distant chains is 1.49 μm. The average distance between vortices within an individual chain varies in the range from 1.05 to 1.30 μm for various chains. Figure 2c shows a part of the vortex array in which chains with a small pitch (0.9 μm) and chains with a large pitch (1.3 to 1.6 μm) alternated. The distances between the chains alternated similarly to the lattice shown in Fig. 2b. Figure 2d shows the small area in which the vortices were least ordered.

Figure 3a shows the vortex structure of the crystal obtained in the scanning electron microscope after exfoliating of the approximately 10 μm thick surface layer and decoration at $T = 18.1$–18.9 K, and $H = 7.3$ Oe (FC). The decoration also revealed chains of well-resolved vortices and, in addition, areas where individual vortices in the line were almost unresolved. In the region where vortices were resolved, the average distance between vortices in chains was 1.6–1.75 μm, and the distance between chains was 1.7 μm.

In the decoration experiments, a superconducting $Bi_2Sr_2CaCu_2O_{8+x}$ single crystal (BSCCO-2212) was used as a reference sample, in which a regular triangular vortex lattice is formed in the FC mode. Figures 3a and 3b show for comparison the vortex lattices on the surface of the investigated crystal $EuRbFe_4As_4/EuFe_2As_2$ and BSCCO, respectively, obtained in the same experiment. The individual vortices on BSCCO

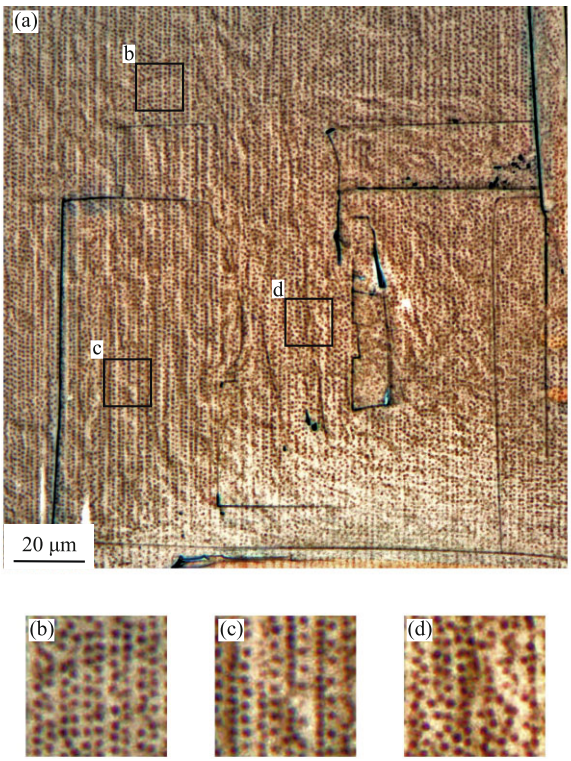

Fig. 2. (Color online) Iron nanoparticles clusters (dark) visualizing the Abrikosov vortices on the sample surface along the reference *ab* plane at $T \approx 8$ K, $H = 15$ Oe. The vortices predominantly are lined up in vertical chains. Dark linear defects are the facet boundaries formed within the surface cleaving. (a) Optical microphoto, magnification ×500. (b–d) The characteristic vortex lattice features, which are discussed in the text. The scale of figures (b–d) is enlarge by a factor three relative to Fig. 2a.

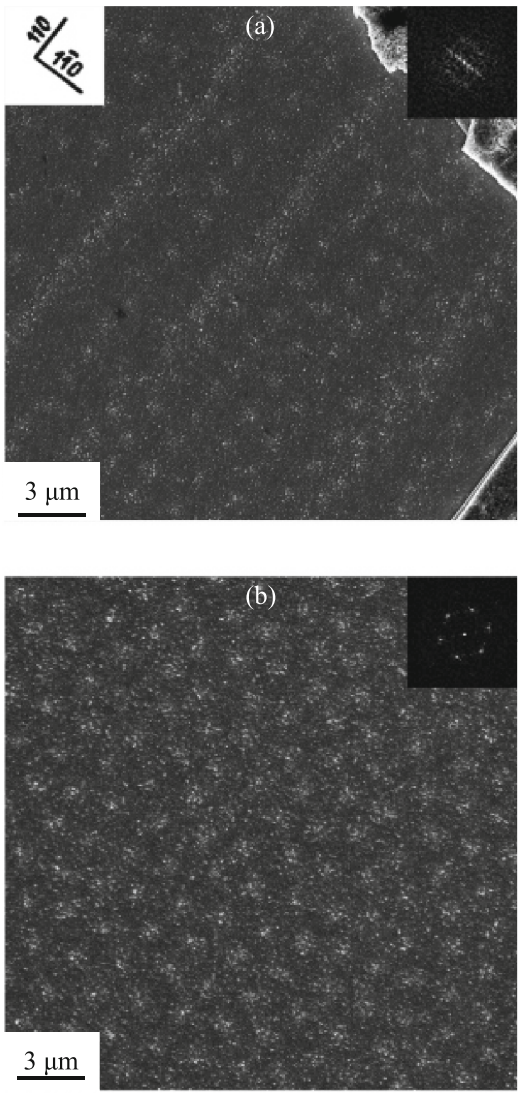

Fig. 3. (a) Abrikosov vortices lattice on the inhomogeneous $EuRbFe_4As_4$ crystal at $T_D \approx 18$ K, $H = 7.3$ Oe (in the left inset shows the crystallographic axes in coordinates of 1144 system). (b) Correct hexagonal Abrikosov vortices lattice on the single crystal BSCCO-2212 surface. Both images were obtained in one experiment. In the right insets show the Fourier images of the corresponding vortex structure (in arbitrary scale units).

were well resolved, with a density of $0.352\ \mu m^{-2}$, which correlates exactly with the external field of 7.3 Oe. The insets show Fourier patterns emphasizing the ordering of vortices into lines (Fig. 3a) and into a triangular lattice (Fig. 3b), as well as the larger intervortex spacing in the investigated crystal than in BSCCO. We note in this image the difference in observed diameter of Abrikosov vortices in $EuRbFe_4As_4$ (≈1.1 μm) and BSCCO (≈1.3 μm).

It should also be noted that further-three exfoliations from the same crystal of surface layers with a total thickness of ~15 μm led to the disappearance of superconductivity in the sample, which was confirmed by the absence of Abrikosov vortices during decoration, as well as the absence of diamagnetic response of magnetic susceptibility $\chi'(T)$ near the temperature of 40 K. Elemental analysis (EDX) after layer exfoliation showed the absence of rubidium on the sample surface, and its atomic composition corresponded to $EuFe_2As_2$. In this regard, it can be concluded that the superconducting phase 1144 formed the near-surface layer of the sample removed by exfoliation, and most of the crystal was the parent phase 122.

The obtained results can be interpreted as follows. The sample studied in this work possesses a linearly ordered vortex structure, which is uncharacteristic of iron-containing superconductors. Previously observed vortex lattices on $EuRbFe_4As_4$ single crystals were disordered due to intrinsic pinning [16]. Figure 4 shows the lattice of Abrikosov vortices on the surface of a single crystal of $EuRbFe_4As_4$ studied in [17], which was grown by solid-phase reaction [13] and had no pronounced features of the $EuFe_2As_2$ phase. The

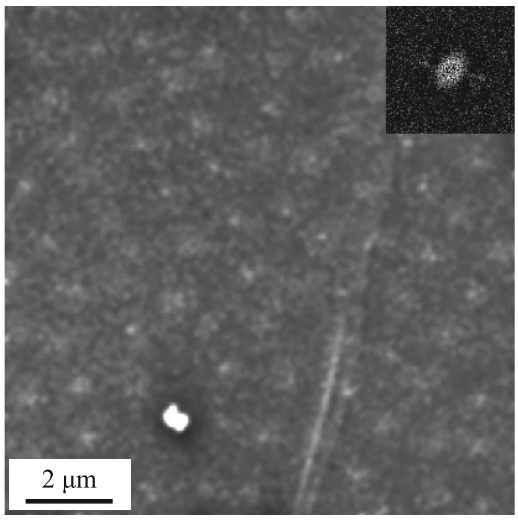

Fig. 4. Abrikosov vortices lattice on the $EuRbFe_4As_4$ single crystal in the absence of the $EuFe_2As_2$ phase with $T_D \approx 8$ K, $H \approx 25$ Oe, and the corresponding Fourier image.

ordering in such a vortex lattice is absent, which is confirmed by the Fourier image.

The linear structure of Abrikosov vortices was observed earlier in superconducting crystals with twinning, in particular in $YBa_2Cu_3O_x$ [18], where such ordering was caused by pinning of vortices at twinning boundaries, and also in superconducting borocarbides [19], in which pinning was caused by strong scattering fields at the boundaries of antiferromagnetic domains coinciding with twinning boundaries [20].

No twin structure was observed in $EuRbFe_4As_4$, in contrast to $EuFe_2As_2$, where it was detected at $T \leq T_{twin} \approx 190$ K by neutron studies in [21] and by direct visualization in [22]. As mentioned above (Fig. 1a), the coexistence of phases 1144 and 122 was initially detected in the studied crystal, and the subsequent removal of the surface layer led to the complete removal of the superconducting phase 1144, which was confirmed by the absence of diamagnetic decrease in magnetic susceptibility near the temperature of 40 K. Thus, it was determined that the superconducting phase 1144 was located only in the near-surface layer ~15 μm thick above the 122 phase and was influenced by the twins of phase 122, as evidenced by the ordering of vortices along the direction $\langle 100 \rangle_T$ coinciding with the direction of twin boundaries in phase 122, as well as the correspondence between the distance between the chains of vortices and the distance between the twin boundaries determined in [22].

Determination of the exact mechanism of vortex pinning in phase 1144 caused by twinning boundaries in phase 122 requires additional studies, but the following assumption can be made. Apparently, twinning of phase 122 leads to mechanical deformation of the thin layer of phase 1144 grown on phase 122. Since the regions of phase 1144 located above neighboring twinning domains are deformed in mutually perpendicular directions (in accordance with the *a* and *b* axis directions of the rhombic phase 122), strong stresses should arise above the twinning boundary, as in phase 122. In such a case, it is in the region of the twin boundaries that the magnetic field will easily penetrate into the superconductor. The stress may result in the formation of real twin boundaries with a suppressed order parameter, as in the case of YBaCuO [23]. The latter assumption requires further investigation involving low-temperature X-ray diffractometry. As an alternative mechanism of vortex ordering, the influence of stray magnetic fields on twin boundaries was considered as in the case of borocarbides [20]; however, when decorating the $EuFe_2As_2$ *ab* crystal plane in perpendicular field without a superconducting phase, twin boundaries were not visualized by either the decoration method or the magneto-optical method [22], in contrast to the work [20], where $ErNi_2B_2C$ and $TbNi_2B_2C$ were studied. This suggests that the stray fields at the $EuFe_2As_2$ twin boundaries are very low and insufficient for appreciable vortices pinning.

In [23], the pinning potential of vortices at the single twin boundary of $YBa_2Cu_3O_x$ crystals with suppressed order parameter was calculated based on the decrease in the intervortex distance a_b at the twin boundary compared to the intervortex distance in the twin volume a_v. An estimation of the pinning potential for this region can be made using the formula from [23]:

$$U_p = \frac{\Phi_0^2}{8\sqrt{2}\pi^{3/2}\lambda^2} \times \left[\left(\frac{a_b}{\lambda}\right)^{1/2} \exp\left(-\frac{a_b}{\lambda}\right) - \frac{3}{2}\left(\frac{a_v}{\lambda}\right)\exp\left(-\frac{a_v}{\lambda}\right)\right],$$

where Φ_0 is the magnetic flux quantum, λ is the magnetic field penetration depth, a_b and a_v are the intervortex distance at the twin boundary and in the twin volume, respectively. With the following assumptions, we can estimate the pinning potential in our case: consider the intervortex distance in chains with a small pitch as a_b, and the intervortex distance in chains with a large pitch as a_v (Fig. 2c). Based on literature data [24] and our estimates of the apparent diameter of the vortex image (Fig. 3) for $EuRbFe_4As_4$ and BSCCO with known penetration depth [25], the penetration depth for $EuRbFe_4As_4$ is assumed to be 130 nm. This estimate gives a value of $U_p \sim 3 \times 10^{-8}$ erg/cm in the field of 15 Oe, which is of the same order of magnitude as the pinning potential in $YBa_2Cu_3O_x$.

In summary, a lattice of Abrikosov vortices was visualized by a low-temperature decoration method using magnetic nanoparticles in an inhomogeneous crystal of an iron-containing superconductor. The

studied sample was a ~15 μm-thick quasi-epitaxial film of the superconducting $EuRbFe_4As_4$ phase on a substrate of the non-superconducting parent $EuFe_2As_2$ phase with twinning. In system 1144, the ordering of vortices into chains was observed for the first time. The chains direction coincided with the direction of the twin boundaries of phase 122, which was attributed to pinning in the mechanically stressed regions of phase 1144 above the twin boundaries of phase 122. The observed ordering of vortices above the twin boundaries can be considered as a way to control the vortex structure, which may find technical applications, for example, in the production of superconducting tapes for magnet coils made of iron-containing superconductors [26]. The influence of the substrate is of independent interest because epitaxial thin-film structures on single-crystal substrates are used for large-scale applications of high-temperature superconductors [27].

ACKNOWLEDGMENTS

The authors would like to thank E.Yu. Postnova for scanning electron microscope work, S.S. Khasanov for discussion of the results, L.G. Isaeva, V.N. Shilov, and A.N. Rossolenko for technical support.

FUNDING

Crystal growth was performed with support of the Russian Science Foundation (project no. 21-13-00307) using the equipment of the LPI Shared Facility Center. The work was partially performed under the state assignment of the Osipian Institute of Solid State Physics, Russian Academy of Sciences.

CONFLICT OF INTEREST

The authors of this work declare that they have no conflicts of interest.

OPEN ACCESS

REFERENCES

1. S. Zapf and M. Dressel, Rep. Prog. Phys. **80**, 016501 (2017).
2. M. P. Smylie, K. Willa, J.-K. Bao, K. Ryan, Z. Islam, H. Claus, Y. Simsek, Z. Diao, A. Rydh, A. E. Koshelev, W.-K. Kwok, D. Y. Chung, M. G. Kanatzidis, and U. Welp, Phys. Rev. B **98**, 104503 (2018).
3. Zh. Devizorova and A. Buzdin, Phys. Rev. B **100**, 104523 (2019).
4. K. Iida, Y. Nagai, S. Ishida, et al., Phys. Rev. B **100**, 104506 (2019).
5. T. K. Kim, K. S. Pervakov, D. V. Evtushinsky, et al., Phys. Rev. B **103**, 174517 (2021).
6. V. S. Stolyarov, K. S. Pervakov, A. S. Astrakhantseva, I. A. Golovchanskiy, D. V. Vyalikh, T. K. Kim, S. V. Eremeev, V. A. Vlasenko, V. M. Pudalov, A. A. Golubov, E. V. Chulkov, and D. Roditchev, J. Phys. Chem. Lett. **11**, 9393 (2020).
7. T. K. Kim, K. S. Pervakov, V. A. Vlasenko, A. V. Sadakov, A. S. Usoltsev, D. V. Evtushinsky, S. Yun, G. Poelchen, K. Kummer, D. Rodichev, V. S. Stolyarov, I. A. Golovchansky, D. V. Vyalykh, V. Borisov, R. Valenti, et al., Phys. Usp. **65**, 740 (2022).
8. A. Yu. Degtyarenko, I. A. Karataev, A. V. Ovcharov, V. A. Vlasenko, and K. S. Pervakov, Nanomaterials **12**, 3801 (2022).
9. J.-K. Bao, K. Willa, M. P. Smylie, H. Chen, U. Welp, D. Y. Chung, and M. G. Kanatzidis, Cryst. Growth Des. **18**, 3517 (2018).
10. M. Tegel, M. Rotter, V. Weiß, F. Schappacher, R. Pottgen, and D. Johrendt, J. Phys.: Condens. Matter **20**, 452201 (2008).
11. M. A. Kuzovnikov, V. E. Antonov, V. I. Kulakov, V. D. Muzalevsky, N. S. Orlov, A. V. Palnichenko, and Yu. M. Shulga, Phys. Rev. Mater. **7**, 024803 (2023)
12. D.-X. Chen and V. Skumryev, Rev. Sci. Instrum. **81**, 025104 (2010).
13. Y. Liu, Y.-B. Liu, Z.-T. Tang, H. Jiang, Zh. Wang, A. Ablimit, W. Jiao, Q. Tao, Ch. Feng, Zh. Xu, and G.-H. Cao, Phys. Rev. B **93**, 214503 (2016).
14. S. Jiang, Y. Luo, Z. Ren, Z. Zhu, C. Wang, X. Xu, Q. Tao, G. Cao, and Zh. Xu, New J. Phys. **11**, 025007 (2009).
15. L. Ya. Vinnikov, I. S. Veshchunov, M. S. Sidel'nikov, and V. S. Stolyarov, Prib. Tekh. Eksp., No. 4, 790 (2022).
16. L. Ya. Vinnikov, A. G. Troshina, I. S. Veshchunov, D. Analitis, I. Fisher, Yu. Liu, C. T. Lin, L. Fang, U. Welp, and W. K. Kwok, JETP Lett. **96**, 655 (2012).
17. V. S. Stolyarov, A. Casano, M. A. Belyanchikov, et al., Phys. Rev. B **98**, 140506(R) (2018).
18. L. Ya. Vinnikov, L. A. Gurevich, G. A. Yemelchenko, et al., Solid State Commun. **67**, 421 (1988).
19. L. Ya. Vinnikov, J. Anderegg, S. L. Bud'ko, P. C. Canfield, and V. G. Kogan, Phys. Rev. B **71**, 224513 (2005).
20. L. Ya. Vinnikov, I. S. Veshchunov, S. L. Bud'ko, P. C. Canfield, and V. G. Kogan, J. Phys.: Conf. Ser. **150**, 052279 (2009).

21. Y. Xiao, Y. Su, M. Meven, R. Mittal, C. M. N. Kumar, T. Chatterji, S. Price, J. Persson, N. Kumar, S. K. Dhar, A. Thamizhavel, and Th. Brueckel, Phys. Rev. B **80**, 174424 (2009).

22. L. S. Uspenskaya, M. S. Sidelnikov, K. S. Pervakov, V. A. Vlasenko, and L. Ya. Vinnikov, J. Surf. Invest.: X-Ray, Synchrotr. Neutron Tech. **18**, 47 (2024).

23. L. Ya. Vinnikov, I. V. Grigor'eva, L. A. Gurevich, and A. E. Koshelev, Sverkhprovodim.: Fiz. Khim. Tekh. **3**, 1434 (1990).

24. D. Collomb, S. J. Bending, A. E. Koshelev, M. P. Smylie, L. Farrar, J.-K. Bao, D. Y. Chung, M. G. Kanatzidis, W.-K. Kwok, and U. Welp, Phys. Rev. Lett. **126**, 157001 (2021).

25. G. Blatter, M. V. Feigel'man, V. B. Geshkenbein, A. I. Larkin, and V. M. Vinokur, Rev. Mod. Phys. **66**, 1125 (1994).

26. D. Wang, Zh. Zhang, X. Zhang, D. Jiang, Ch. Dong, H. Huang, W. Chen, Q. Xu, and Y. Ma, Supercond. Sci. Technol. **32**, 04LT01 (2019).

27. A. A. Thomas, I. A. Shipulin, S. Holleis, M. Eisterer, K. Nielsch, and R. Huhne, Supercond. Sci. Technol. **34**, 115013 (2021).

Translated by the authors